Journal of Molecular Graphics and Modelling 46 (2013) 83–92

Contents lists available at ScienceDirect

Journal of Molecular Graphics and Modelling

journal homepage: www.elsevier.com/locate/JMGM

Stepwise design of non-covalent wrapping of large diameter carbon nanotubes by peptides

Xin Chen*, Xiaohan Yu, Yafang Liu, Jinglai Zhang

Institute of Environmental and Analytical Sciences, College of Chemistry and Chemical Engineering, Henan University, Kaifeng 475001, Henan, China

ARTICLE INFO

Article history:
Accepted 30 September 2013
Available online 10 October 2013

Keywords:
Non-covalent functionalization
Single-walled carbon nanotubes (SWCNTs)
Peptide
Molecular design
Molecular dynamics

ABSTRACT

Single-walled carbon nanotube (SWCNT) is one of the most popular low-dimensional carbon materials in material science, nanomedicine, and nanoscale electronics. Yet the application of the SWCNTs was hindered by the self-aggregation. To purify and disperse the SWCNTs, non-covalent wrapping is one of the effective options to overcome such defects. In this work, two kinds of short peptides were designed to facilitate the modification of large-diameter SWCNT. The design of the peptide was carried out in a stepwise manner. The effective residues of helix-rich and sheet-rich proteins on SWCNT were studied at the first step, and then a coarse model peptide composed of the key adsorption residues above was built to investigate the adsorption dynamics on SWCNT. In the end, the residues include long alkyl side chain and that include aromatic rings were found to play key roles on the adsorption of protein/peptide on hydrophobic SWCNT. And two peptides rich in the long alkyl chain and aromatic rings were constructed respectively. The predominant adsorption capabilities of the two kinds of peptides were discerned by the adsorption details.

1. Introduction

Nanoparticles are highly promising candidates in many important biological applications, such as biomaterials [1], biosensor development [2,3], biomedical devices [4], and cellular delivery of peptides and proteins [5,6]. Since the discovery of carbon nanotubes (CNTs), they have raised considerable attention due to their fascinating structures and properties. However pristine CNTs are highly hydrophobic, the main obstacle in the utilization of CNTs in biological and medicinal chemistry is their poor solubility in aqueous-based biological milieu. The reason of the phenomenon is that the CNTs themselves are easy to aggregate and lead to the toxicity in the organisms. In order to improve the medicine carrying performance and reduce the toxicity of the CNTs, biomolecular functionalization has been found to be one effective option to overcome such defects. Meanwhile, the interaction between nanomaterials and biosystems is of great significance and practical interest, which determines the biocompatibility and the potential utilities of nanomaterials in biological settings [2–4]. Especially single-walled carbon nanotubes (SWCNTs), which are hollow cylinders formed by seamlessly wrapping a single graphene sheet. They are characterized by a pair of integers (n, m) called the chiral vector which is the graphene sheet translation vector defining the axial direction of the nanotube [5]. Because of the extraordinary electrical and mechanical properties, SWCNTs are applied in various biotechnology fields and have recently started to emerge and raise great hopes. Unfortunately, pristine CNTs are toxic mainly due to the insolubility and aggregation as a consequence of high hydrophobicity [6,7]. Then SWCNTs are difficult to be purified and separated, and hence difficult to be assembled into useful structures. Although the lack of solubility of CNTs in aqueous media limits their application in bio-nanosystems, recently both covalently [8] or non-covalently [9] functionalized CNTs are instead highly soluble in aqueous biological media and thus have been widely used in biological fields [6,10]. The non-covalently [9] functionalized CNTs is increasingly developed because it could preserve the native structure and functional properties of SWCNTs. The water solubility of CNTs with non-covalent modifications is clearly improved and their biocompatibility profile is completely transformed. The non-covalent functionalizations of CNTs are focused on the bundle of long chain biomolecules with CNTs. For example, the surfactant molecules [11], conjugated polymers [12], DNA [13], peptides [14] and proteins [15] are widely used to wrap and disperse the CNTs. Dieckmann et al. have designed a 29-residue peptide, named nano-1, which can fold into an amphiphilic α-helical conformation, interact with the aromatic surface of SWCNTs, and disperse them in aqueous solution [16]. The Raman spectroscopic, atomic force microscopy (AFM) and transmission electron microscopy (TEM) images have shown that the SWCNTs are indeed

* Corresponding author.
E-mail addresses: xin.chen@henu.edu.cn (X. Chen), zhangjinglai@henu.edu.cn (J. Zhang).

1093-3263/$ – see front matter © 2013 Elsevier Inc. All rights reserved.
http://dx.doi.org/10.1016/j.jmgm.2013.09.012

wrapped by the peptide in aqueous solution and are dispersed with a diameter range from 0.7 nm to 3.3 nm [17–19]. Chiu et al. [20,21] have used fully atomistic molecular dynamics (MD) simulations to investigate the molecular details of nano-1 at three different water/hydrophobic interfaces. It was found that the peptide conformation especially its secondary structure at the various hydrophobic surfaces has the different unfolding state. Zuo et al. [22] have used large-scale MD simulations to study the interaction between several proteins and carbon nanotubes. It was found that the CNT can plug into the hydrophobic core of proteins to form stable complexes. Wang et al. [23] have used explicit solvent molecular dynamics simulations to investigate the dynamics and mechanism of the adsorption of the model peptide on different charged SWCNTs. And Wu et al. [24,25] have studied the spontaneous encapsulation of a globular protein into the CNT with different tube size. It was proved that the protein makes a stepwise conformational change to maximize its affinity to the CNT walls as well as the protein–CNT interaction during the insertion.

From the previous investigations, it could be confirmed that the protein/peptide wrapping was an effective strategy to modify the biocompatibility of CNTs. However, the modification of CNTs is mainly focused on the small-diameter CNTs. As is known to all is that large-diameter CNTs can be used to package the medicine and carry the larger biomolecules. The dispersion and the modification of the biocompatibility of large CNTs are also important for the CNT-related drug carrier design. Considering the difficulty and restriction of the wrapping with protein/peptide on large-diameter CNTs, a kind of solution composed of short peptides were introduced for the non-covalent modification of CNTs. For the preparation, the short peptide is easy to get and readily to be adsorbed on CNTs. In the body, the short peptide is safe and can be adsorbed naturally at a manageable pace. The design of peptide is begun from the study of helix-rich and sheet-rich proteins with SWCNTs. We have selected insulin which is rich in α-helix and the WW domain which is rich in β-sheet as the model proteins. And the functional peptide will be constructed by the key adsorption residues which are found in the two proteins.

In this work, two typical short peptides with 22-residues were designed for the modification and dispersion of large SWCNTs. The design was dependent on the study of dynamical mechanisms between the protein rich in helix or sheet and SWCNT. Different from the design of nano-1, the peptide referred in this work was used to design a kind of peptide that was facile to be prepared and effective on the modification of large-diameter SWCNTs. Local features, including characteristics of the different amino acid side groups, orientation and reorientation of the protein/peptide on the interface are essential for the understanding of the mechanism of protein adsorption on heterogeneous surfaces, and the significance of the secondary and tertiary structural evolution of the protein for the systems is also of concern. All these details are studied with atomistic simulations in this paper.

2. Methods and materials

2.1. System setup

The X-ray structures of insulin and WW-domain (shown in Fig. 1) were obtained from the Protein Data Bank with the PDB ID codes: 2GF1 and 1E0M, respectively. Insulin is an important peptide hormone, which regulates the metabolism of glucose, and the detection of insulin is of great importance for clinical diagnostics. It is a 70-residues peptide and mainly composed of three α-helices. The WW domains are signaling and regulatory proteins used as functional modules to identify and bind to the praline-rich motifs (PRMs) [26]. And the 37-residues WW domain used in this paper

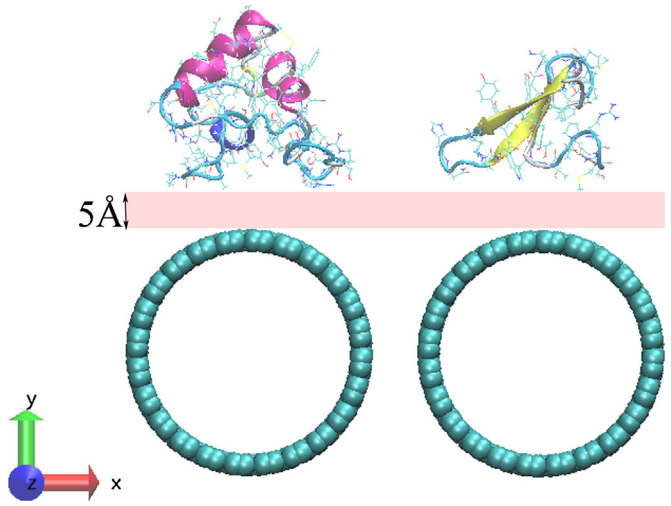

Fig. 1. Schematic view of the initial structures of (a) insulin and (b) WW domain on the armchair (24, 24) SWCNT surface. The water molecules were omitted for clarity. The model proteins are displayed by cartoon model. The axial direction of the CNT surface was set to be parallel to the *z*-direction.

was composed of three anti-parallel β-sheets. The initial coordinates of single-walled CNTs were generated using the nanotube builder plug-in of VMD package [61]. The armchair (24, 24) SWCNT with the diameter of 3.254 nm was constructed in this work. The length of SWCNT is approximately 80 Å with 33 cell replications. The carbon atoms of SWCNT were modeled as the uncharged Lennard–Jones particles reporting on biomolecule–CNT interaction in large amount of literatures [27–31], and it was also employed in this work. The model proteins were put on the surface of (24, 24) SWCNT with the distance of 5.0 Å. A series of orientations of model proteins were considered to put on the surface of SWCNT, and the most favorable one shown in Fig. 1 was discussed in this paper. Both the two protein-SWCNT systems were solvated with SPC model [32,33] water boxes with the sizes of 44.49 Å × 78.69 Å × 91.79 Å and 44.49 Å × 72.63 Å × 91.80 Å, respectively.

2.2. MD simulation details

In this work, all of the MD simulations were performed in the isothermal-isobaric (NPT) ensemble with NAMD 2.7b [34]. The Charmm27 all-atoms force field [35] was used. The force field parameters of carbon nanotubes were obtained from reference [36] and all the carbon atoms of SWCNT were set to be neutral. And counterions (sodium and chloride ions) were added to neutralize the system. The parameters of Lennard–Jones potential for the cross interactions between non-bonded atoms, such as CNT-protein, CNT-water were obtained from the Lorentz–Berthrlot combination rules as in many researches [37–40]. A time step of 2 fs was set and the cutoffs of the VDW force was implemented by a switching function starting at a distance of 10 Å and reaching zero at 12 Å. Particle mesh Ewald (PME) summation was used to calculate the long-ranged electrostatic interactions, with a cutoff distance of 12 Å for the separation of the direct and reciprocal space. Periodic boundary conditions were employed with a solvent shell of 8 Å for all the simulations. During the MD simulations, Langevin method was employed to keep the temperature constant at 310 K and the pressure at 101.3 kPa. The axial direction of the CNTs was set to parallel to the *z*-axis. Thus the cross sections of the CNTs were in the *x*–*y* plane. All carbon atoms of the CNT were fixed and the proteins were relaxed in the simulation.

The systems (containing CNTs, model proteins, and water molecules) were first applied for 5000 steps of energy

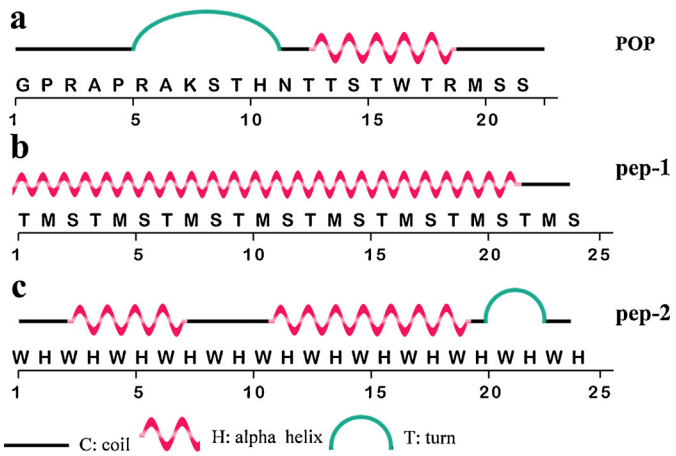

Fig. 2. Schematic view of the first and secondary structures of designed peptides (a) POP, (b) pep-1, and (c) pep-2.

minimization. Then all the systems were carried out for 10 ns MD runs until the root-mean-square deviation (RMSD) and the total energy of protein converged, which indicated that a meta-stable state had been reached. In general, the adsorption of a single peptide/protein molecule on material surface may be a millisecond process, which has to be carried out by coarse-grained or non-equilibrium simulation. In addition, the initial orientation and distance of the peptide probably influence the adsorption process. Long-time and multiple MD simulations could overcome these drawbacks [41,42]. However, the literatures [29,37,38,43] showed that all-atom simulations of adsorption of protein could provide sufficient and useful information for the meta-stable structure in nanosecond scale.

2.3. Design of functional peptides

There were many factors working on the formation of SWCNT adducts in the solution of protein/peptide, such as the rigidity of protein, the pH, the temperature, the edge effects, the orientation of biomolecules, the size of CNT, and the assimilation by the body [22,44–47]. Based on the design of nano-1, we focused on the modeling of more applicable and facile peptides to modify and disperse the large size SWCNTs. First, the adsorbed residues found from the insulin and WW domain were summarized to construct a 22-residues peptide chain by the PEP-FOLD [48–53], and it was named POP. POP was put into the water box to be equilibrated for 10 ns and then the equilibrium structure of POP was put on the surface of SWCNT (24, 24) for 10 ns MD simulation, and the effective residues were classified again. Secondly, the two most effective adsorption peptides (pep-1 and pep-2) were constructed by these effective residues selected above. And the equilibrium MD simulation of peptides and peptide-SWCNT composite in water box would be performed for 10 ns.

The new peptide POP was composed of non-polar residues, long chain residues, and the aromatic residues, which was easy to be adsorbed on the surface of SWCNT. The amino acid sequence of POP was set to be GPRAP RAKST HNTTS TWTRM SS. It was consisted of one helix and two loop structures (Fig. 2). The helix was composed of the residues from Thr13 to Arg19 and one of the loop structures was composed of the residues from Gly1 to Asn12, then the other loop included residues Met20, Ser21 and Ser22. The new designed peptide POP was also immersed in the periodic water box and performed MD simulation for 10 ns to equilibrate the system.

The long alkyl chain-rich and aromatic ring-rich peptides were named as pep-1 and pep-2, respectively. As shown in Fig. 2, the amino acid sequence of pep-1 was set to be TMSTM STMST MSTMS TMSTM STMS. It was mostly composed of α-helix (Thr1 to Ser21). And the sequence of pep-2 was set to be WHWHW HWHWH WHWHW HWHWH WHWH. It was consisted of two α-helices (Trp3 to Trp7, Trp11 to Trp19) and they were connected with loops.

2.4. Analytical methods

The time-dependent interaction, $E_{\text{int}}(t)$, for all the systems in MD simulations are defined as follows:

$$E_{\text{int}}(t) = E_{CNT+PRO}(t) - E_{CNT}(t) - E_{PRO}(t) \quad (1)$$

In Eq. (1), $E_{\text{int}}(t)$ stands for the total interaction between the model protein and the CNT surface at time t during the MD simulation, and $E_{CNT+PRO}(t)$, $E_{CNT}(t)$ and $E_{PRO}(t)$ are the total potential energy of the CNT–protein complex, the potential energy of CNT and that of the protein at time t during MD simulations, respectively. The definition of VDW interaction energy and the electrostatic interaction energy are same as to the potential interaction energy [29,37]. This protocol has been successfully applied in the investigation of the peptide/protein adsorption and desorption in inorganic material surfaces [29,37,38,43].

The contact area between the protein and the CNT is calculated as:

$$A_{contact}(t) = \frac{1}{2}(A_{PRO} + A_{CNT} - A_{CNT+PRO}) \quad (2)$$

where A_{PRO} is the molecular surface area for the entire protein/peptide, A_{CNT} is the corresponding surface area for the nanotube, and $A_{PRO+CNT}$ is the surface area of the protein/peptide-nanotube complex. Surface areas were calculated using the SASA plug-in of VMD [20,21,54] and it was calculated with the probe radius of 1.4 Å.

The π–π stacking interactions are incorporated into the VDW dispersion interaction in classical force fields and are geometrical in nature [55,56]. The distances between the centers of the residues which have the aromatic rings and the surface of the nanotube are analyzed to characterize the π–π stacking orientation of the residues with aromatic rings with respect to the nanotube sidewall [20,21].

3. Results and discussion

3.1. Equilibrium simulation

MD simulations of 10 ns for each system were carried out to release the rearrangement of protein on the surface of SWCNT. The potential energy, RMSD and radius of gyration (R_g) of proteins during the simulation were shown in Fig. 3 to illustrate the structural change of the proteins during the adsorption onto CNTs, and they were widely used as the criterion of equilibrium [57,58]. Proteins were pulled and spread on the surface by the attraction of SWCNT. The potential energy and R_g of insulin were gradually decreased with the simulation time, which showed that insulin was rearranged to a more compact and stable conformation. While the RMSD increased with the structural adjustment of insulin from the initial state. All the three curves converged during 10 ns, and it could be concluded that the complex of insulin and SWCNT had reached an equilibrium state. When the WW domain was close to the SWCNT surface, the R_g of WW domain (Fig. 3b) decreased. Yet it was elevated with the protein spreading on the interface. The potential energy of WW domain was kept stable during the whole simulation. And the platform in RMSD curves showed that the system had been equilibrated.

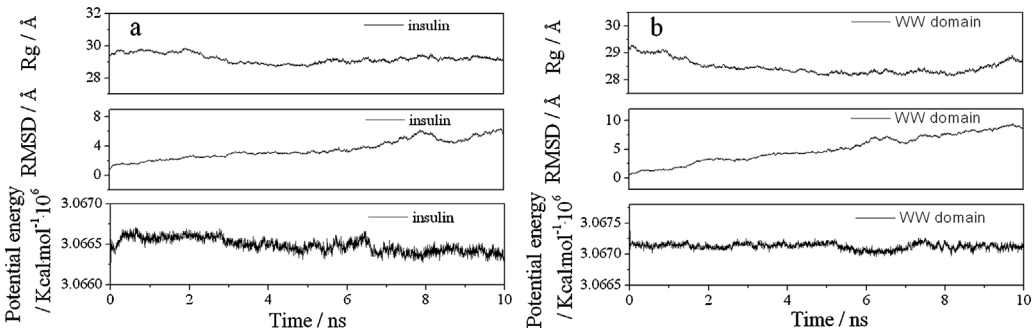

Fig. 3. Time evolution of potential energy, RMSD and R_g of (a) insulin and (b) WW domain.

3.2. Effective adsorption

In 10 ns MD simulations, the adsorption phenomena were observed in all the systems and reflected by the trajectory animation of every simulation. To clarify the adsorption residues of protein on the SWCNT surface, the normalized distance of the center-of-mass of protein to the tube wall (denoted as CMW distance in the following) [29], d/d_0, was employed in this work. Here, the variable d represents the distance of the center-of-mass of the proteins to the tube wall of the CNT, and d_0 is the initial value of d before the MD runs. It is apparent that the trend of the CMW distance in the two systems was gradually decreased, despite some small fluctuations in this process. The small plateaus in the CMW curve (Fig. 4) were resulted by the self-adjustment of the protein conformation, which was induced by the attraction of SWCNT. In other words, it is necessary for the different proteins to adjust themselves to match the geometry of the surfaces, which is helpful to overcome the energy barrier and achieve stronger attraction from the SWCNT. Despite both the two CMW distances were decreased in the simulations, the decline of CMW distance of WW domain was obviously faster and larger than that of insulin. It was showed that WW domain was more readily to be adsorbed on the SWCNT.

The interaction energy between protein and graphite was plotted as a function of the number of residues which were less than 5 Å from the surfaces in Raffaini's simulations [59,60]. In this work, the adsorbed residues within 5 Å of SWCNT were illustrated in Fig. 4 with Licorice model by VMD. It was obvious that the number of adsorbed residues in WW domain system was more than that in insulin system.

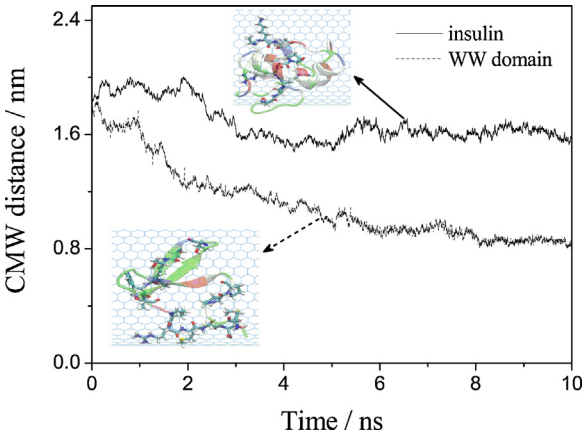

Fig. 4. Normalized distance of center-of-mass of proteins to the tube wall of CNT (denoted as CMW distance) for the two systems. Top views of adsorbed state of insulin and WW domain at the end of simulation were inserted in the graph. Proteins were displayed with cartoon model and the adsorbed residues were highlighted with Licorice model.

3.3. Adsorbed residues

To get more insight into the adsorbed states, the adsorbed residues and interaction energy of protein and SWCNT were presented in Table 1. The number of adsorbed residues in insulin and WW domain was 9 and 14, respectively. In Zuo's study [22], there were nine residues in the second and third β-strands that bind to the SWCNT, with most of them hydrophobic residues such as Trp39. In our work, fourteen residues in the WW domain were found to bind to the SWCNT surface and the Trp appeared three times. At the same time, it was also shown in Wang's study that there were twelve residues (including Phe, Gln, His, Leu, Val, Tyr, Glu, Arg, Lys, and Thr) of insulin adsorbed on the surface of the SWCNT [23]. In this paper, there were only nine residues found to adsorb on the SWCNT surface. The residues Arg and Lys appeared both in Wang's and our study. However, residues Pro, Ser, and Ala had been found in our work, which were not detected in the study of Wang. It was found that the non-polar residues of insulin are in the majority, while the number of polar residues is more in the WW domain system. Moreover, the residues with aromatic rings such as Pro39 in insulin and Trp30 in WW domain were found to play key roles on the adsorption of proteins onto the surface of SWCNT. In the final state, the aromatic rings in these systems tended to be parallel to the CNT surface, which resulted in the maximum contact area of the aromatic rings with the surface. And then it achieved the maximum interaction with the CNT [61]. In addition to the VDW attraction and the hydrophobic interaction between protein and SWCNT, the π–π stacking formed between the aromatic ring and side wall of SWCNT could also drive the phenyl to be parallel to the nanotube [62,63] and cause the high affinity of the proteins to the SWCNT. It was also found that the methylene chain of Lys68 of insulin tended to be exposed to the surface of the SWCNT, which was resulted by the VDW interaction. And this kind of interaction was the main driving force to pull the polar and charged residues to the neutral SWCNT. Then the major interaction between the proteins and the surface were found to be VDW attraction, as well as π–π stacking. Moreover, the initial and final states of insulin and WW domain on the SWCNT surface were shown in Fig. 5. It could be obviously observed from the side view that the adsorbed residues were mainly composed of basic (blue), non-polar (gray) and polar (green) residues. Both the two proteins moved close to SWCNT, and the residues in the interface rearranged to fit the curving surface of SWCNT.

3.4. Structural evolution of protein

During the adsorption process, part of the activity of protein might be lost due to the structure deformation, which had also been observed in some experiments [64,65]. Dutta et al. had found that

Table 1
Adsorbed residues on the SWCNT surface and the values of different kinds of interactions between protein and SWCNT.

System	Adsorbed residues	$E_{int}(VDW)$ (kcal mol^{-1})	$E_{int}(Elec)$ (kcal mol^{-1})	$E_{int}(Total)$ (kcal mol^{-1})
Insulin	Ser34,Ser35,Arg36,Arg37,Ala38,Pro39,Ala67,Lys68, Ser69	−32.4	–	−32.4
WW domain	Met2,Pro5,Pro6,Thr25,Thr27,Ser28,Thr29,Trp30,Thr31,Pro33,Arg34, Met35,Ser36,Ser37	−61.0	–	−61.0

albumin underwent structure deformation when it was adsorbed onto CNT surfaces. To elucidate the structural evolution of helix and sheet on the adsorption process, RMSD of the individual secondary structure was discussed. As shown in Fig. 6a and b, the RSMD of three helices and three sheets was compared with that of the backbone of the whole protein. It is obvious that the RMSD fluctuations of α-helices and β-sheets are smaller than that of the whole protein, especially for α2, α3, β1, β2 and β3, which were kept within 2 Å at most of the simulation time. The RMSD of the helix α1 (Fig. 6a) in insulin was a little higher than that of the other two helices. Further observation on the dynamics of insulin had found that it was resulted by the extending of α1. For the WW domain system, β1 (Fig. 6b) was the most stable structure and it remained on a rather stable value at 2.035 Å. While a sudden rise of the curves of β2 and β3 appeared at 7.5425 ns and 5.2675 ns, respectively. Then all the three curves were overlapped together and kept steady until the end of simulation. The β2 and β3 were close to the surface of SWCNT and they rearranged by the attractive force of SWCNT.

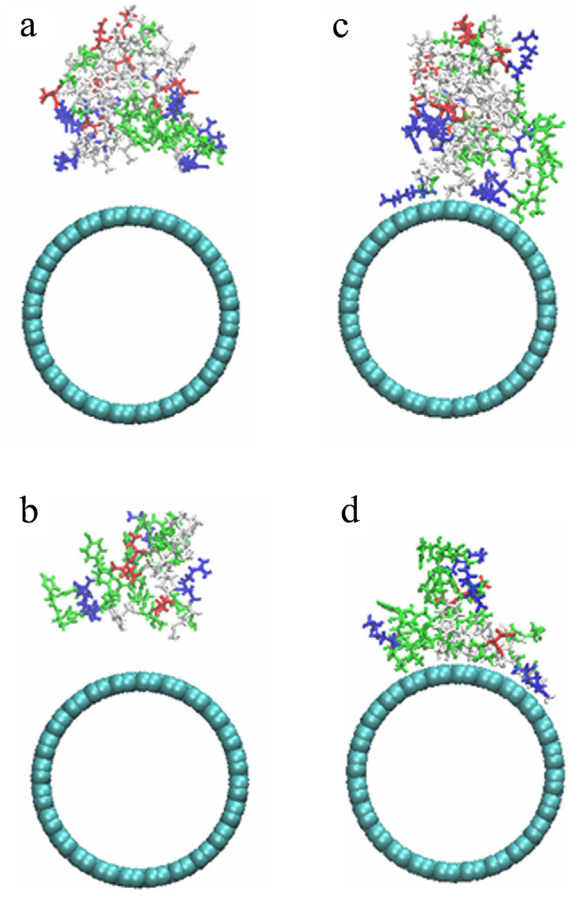

Fig. 5. Side view of the initial state of (a) insulin and (b) WW domain before MD simulations. Side view of adsorbed state of (c) insulin and (d) WW domain on SWCNT surface at the end of MD simulation. Proteins were colored with the property of residue in Licorice model, and SWCNT was colored in cyan with VDW model. The basic, acidic, non-polar and polar residues were colored with blue, red, gray and green, respectively.

The notable high RMSD value of the whole protein indicated that the loose structures (coil and turn) being connected these secondary structures underwent a relatively large deformation upon the adsorption of proteins. The large fluctuation of the tertiary structure of protein was mainly caused by the large deformation of the coils. As shown in Fig. 6c and d, the contents of coil and turn were reciprocal. Yet the contents of helix and sheet were kept stable on a certain value with some ridges and troughs. The coils and turns were gradually attracted to be close to the surfaces. Simultaneously, the helix and sheet were pulled toward the SWCNT until the stable adsorption was formed. The phenomenon could also be proved by the decrease of the distance of CMW as well in Fig. 4.

3.5. Dynamics of protein adsorption

In order to further investigate the dynamics of the adsorption process, the total interaction energy, the VDW interaction energy, and the electrostatic interaction energy between the model proteins and SWCNTs were calculated in Fig. 7. It was found that all the curves of total energy (black) and VDW energy (orange) followed a decreasing trend, which implied the effective interaction between the proteins and the surfaces. Furthermore, the value of VDW interaction was quite similar to the total interaction energy. Yet the electrostatic curves (green) remain on a rather stable value at 0 kJ mol^{-1}, which showed that there was no electrostatic interaction between protein and neutral SWCNT. In other words, the main attractive force was the VDW interaction between protein and SWCNT.

There were some flats and barriers in the VDW curve, which was resulted from the rearrangement of proteins to adapt the curving of SWCNT. The curves indicated a stepwise adsorption dynamics of the two model proteins. From the trajectory animation of the MD simulation, adsorption was always accompanied with the conformational rearrangement and reorientation of the residues that are close to the surfaces, which resulted in the multi-plateaus of VDW interaction curve. Instead, the protein might overcome an energy barrier after conformational change, and then some residues moved gradually closer to the surfaces and were finally kept within approximately 5 Å from the tube wall.

For instance, the total interaction in the WW domain system (Fig. 7b) decreased from −10.73 kcal mol^{-1} to −17.73 kcal mol^{-1} between 1.515 ns and 2.5 ns. It was mainly attributed to the adsorption of Met35, Ser36 and Ser37. The residues exposed to the SWCNT surface was readily to spread on the tube wall, which resulted in the maximum contact area. As shown in the side view of the major residues in the system during the 1.515 ns and 2.5 ns in Fig. 7b, the orientation of the residues Met35 and Ser36 changed from vertical to parallel to the tube wall and then all the three residues lied on the SWCNT to form effective adsorption. Similarly, the total interaction decreased from −18.38 kcal mol^{-1} to −25.54 kcal mol^{-1} from 3.3 ns to 3.7325 ns, and the 7.16 kcal mol^{-1} energy drop was produced by the spread of the side chain of Lys26 on the tube surface. The favorable orientation of Lys26 (Fig. 7b) on the surface led to more hydrogen atoms exposed to the tube wall, which enlarged the VDW interaction of protein and SWCNT. At the same time, other parts of the protein still exhibit the trend to move closer to the surfaces. Also at about 7.5 ns, a big fall of the total interaction was observed from the graph. The 23.53 kcal mol^{-1} energy drop occurred from

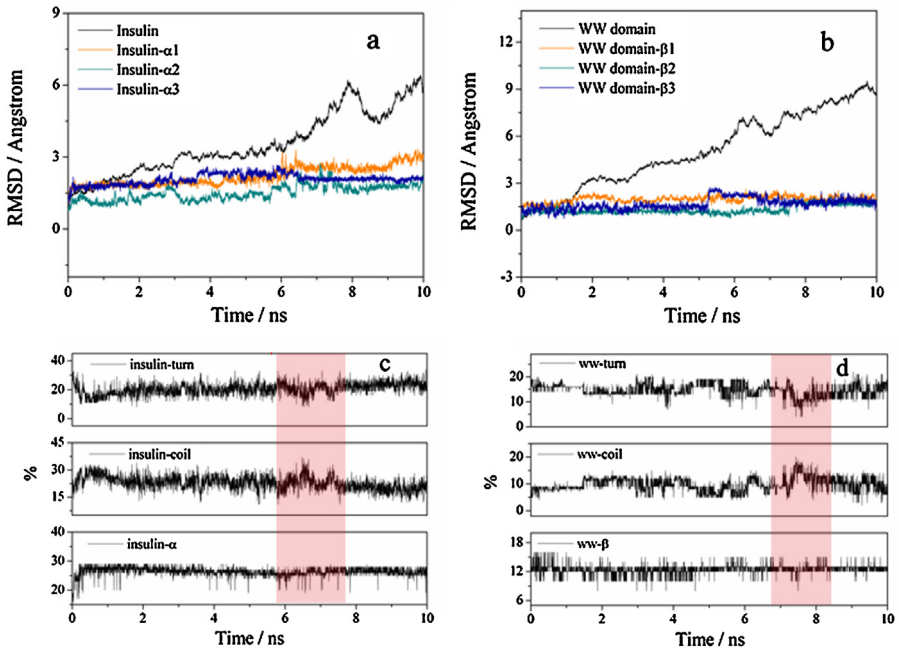

Fig. 6. RMSD of (a) insulin and its individual α-helices α1, α2, α3 and (b) WW domain and its individual β-sheet β1, β2, β3 with respect to the MD time. Content of α-helix, coil and turn in (c) insulin system and content of β-sheet, coil and turn in (d) WW domain system versus MD time.

7.275 ns to 8.125 ns, which was mainly resulted by the moving of the loop (Thr31-Ser37 and Ser1-Pro6) toward the SWCNT (Fig. 7b). Then Met2, Pro5 and Pro6 formed stable adsorption on the surface of SWCNT. The local interaction of protein and SWCNT also influenced the orientation of the whole protein. It was found that the three β-sheets turned with the adsorption of WW domain on SWCNT, which was also discerned by the decline of CMW distance in Fig. 4a.

As discussed above, the conformation and orientation of the protein were induced by the properties and the texture of the surfaces. In other words, protein could adjust its conformation and orientation to fit the arrangement of carbon atoms in the surfaces of SWCNT. After overcoming the energy barrier caused by the conformational rearrangement, one or more residues which had an affinity to the surfaces could be readily adsorbed and make the interaction progress to the next step and finally achieved a relatively stable state.

3.6. Design of peptide

Six orientations (six faces of the hexahedron box) of POP were used to put on the surface of SWCNT and three parallel simulations with the same initial state were performed. Two notable adsorption paths of POP with the same initial state were shown in Fig. 8a and b, respectively.

It could be found from Fig. 8a that POP-a was gradually attracted to the surface of SWCNT in a stepwise manner. The interaction energy showed that three adsorption steps were occurred in the MD process, which was corresponding to the adsorption of 3.75 ns, 6.3 ns and 8.4 ns. The contact area of POP-a was highly consistent with the interaction curve. And the decrease of CMW also illustrated the effective adsorption of POP-a on the SWCNT surface was formed. For the other adsorption path of POP-b, the adsorption was formed in a fast manner. As shown in Fig. 8b, the fast adsorption began from 8.35 ns and reached the stable state at the end of simulation. The curves of interaction energy and contact area were kept rather stable before the adsorption began. While the fluctuation of CMW showed that the conformation of POP-b was rearranged to adapt the SWCNT surface. Once the appropriate conformation

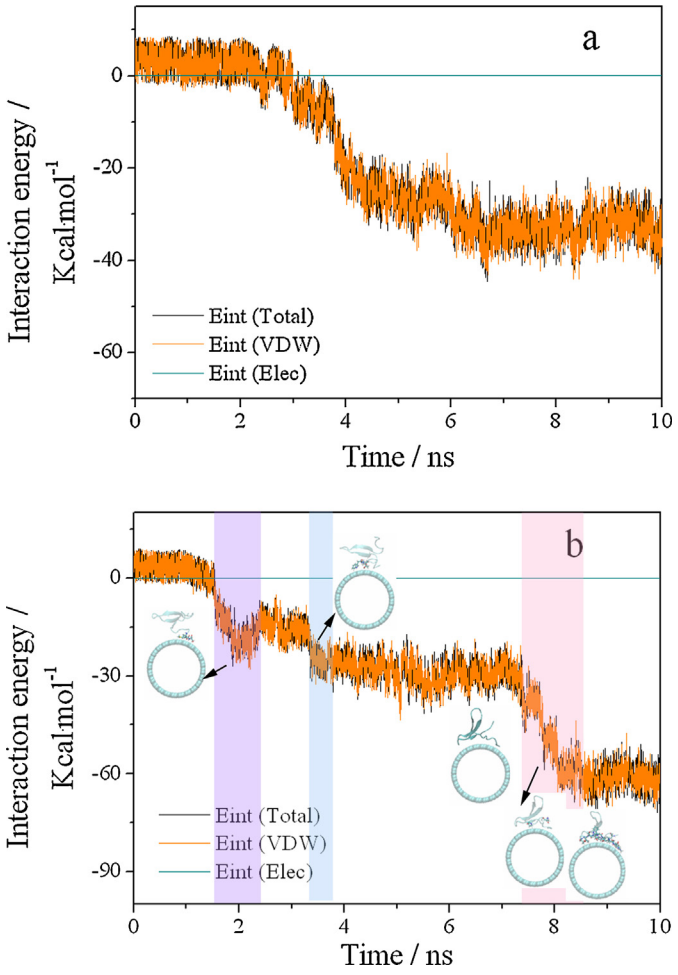

Fig. 7. Total (black), VDW (orange) and electrostatic (dark green) interaction energy between SWCNT and (a) insulin and (b) WW domain during the MD simulation. The side view of the adsorption states of the WW domain during the simulation was also inserted in the graph. (For interpretation of the references to colour in this figure legend, the reader is referred to the web version of this article.)

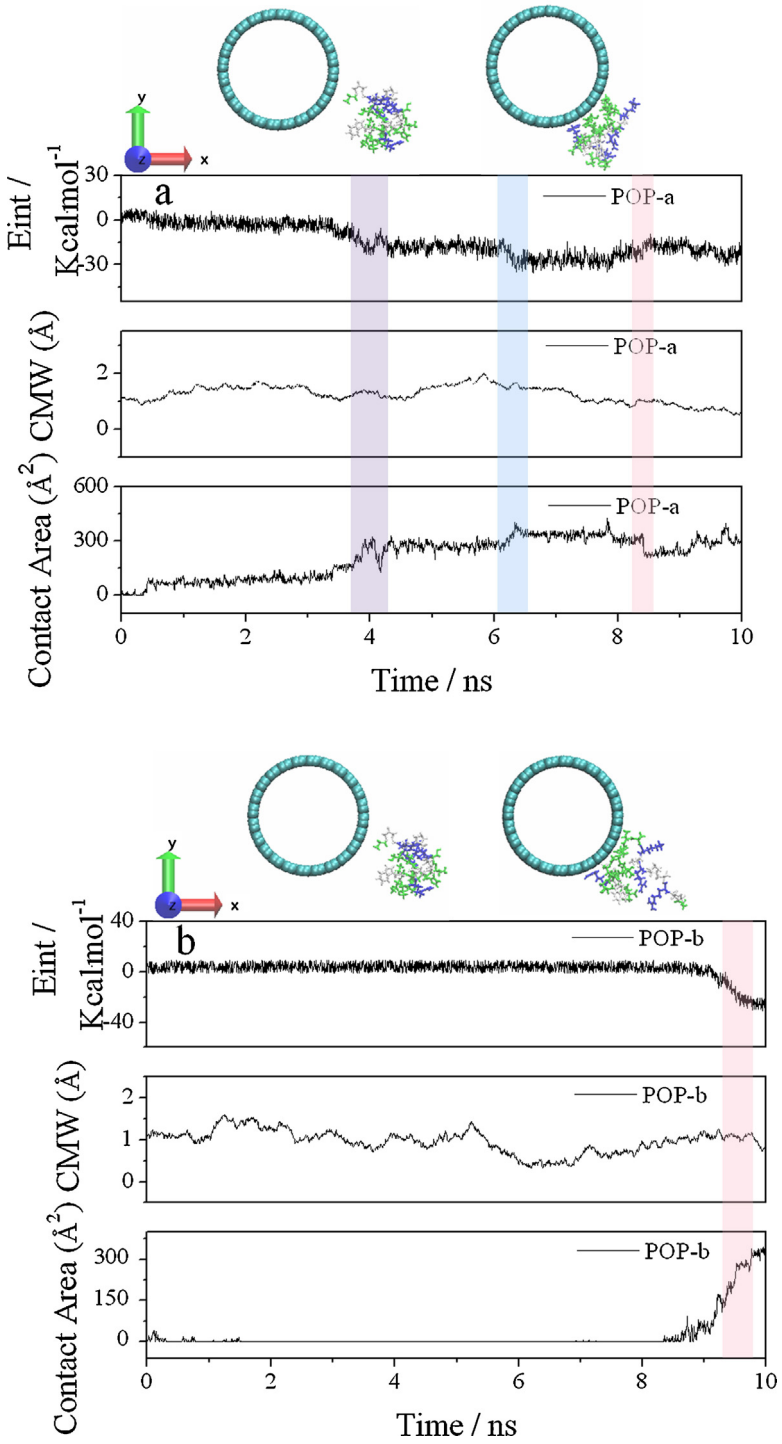

Fig. 8. The interaction energy, CMW distance and contact area between the CNT and (a) POP-a and (b) POP-b in MD simulation. Side view of the initial states (left) and the final adsorption states (right) of POP-a and POP-b. The peptides and the CNT were displayed in Liquorice model and VDW model, respectively. The basic, acidic, non-polar and polar residues were represented with blue, red, gray and green, respectively. Water molecules are not displayed here for clarity. (For interpretation of the references to colour in this figure legend, the reader is referred to the web version of this article.)

of POP-b was completed, the adsorption of POP-b on the SWCNT would be completed quickly. For the POP-a, three adsorption steps were shown with colorful bar in the curves of Fig. 8a. From the trajectory analysis, it could be found that the loop residues Gly1, Pro2, Ala4, Met20, Ser21 and Ser22 were easily adsorbed onto the CNT at the beginning of the simulation. The first adsorption step appeared from 3.41 ns to 4.5 ns was highlighted by the purple bar. In this period, the residue Asn12 came close to the surface of the CNT at 3.41 ns and the whole peptide was pulled onto the CNT surface. At the same time, the residues of the helix spread on the CNT completely, which increased the interaction between the insulin and CNT. The second adsorption step happened from 6.21 ns to 6.42 ns with the complete unfolding of helix. However, the POP was moved on the surface from 8.2 ns to 8.5 ns and helix was partly refolded

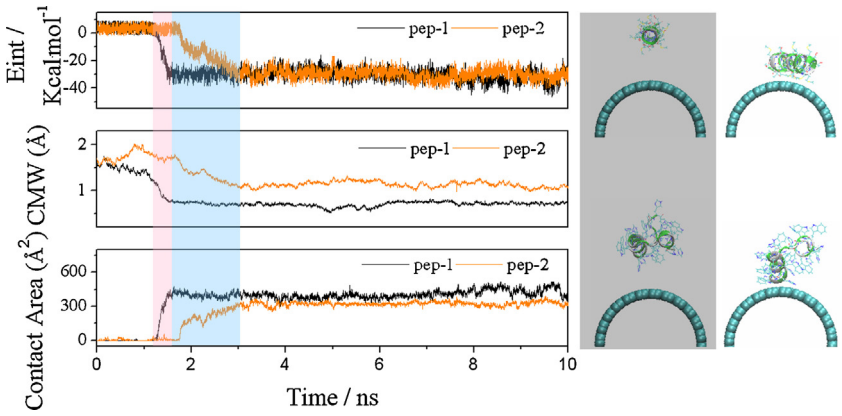

Fig. 9. The interaction energy, CMW and contact area changes of the two peptides adsorbed on the CNT during MD simulation, respectively. Side views of the initial state (gray bar in left) and the final state (in right) of the two peptides pep-1 and pep-2 in the MD simulation.

during the rearrangement of POP on the surface. It was found that POP was partly folded to the unstable π-helix and it unfolded again at the end of simulation.

The other MD trajectory of POP-b was analyzed in Fig. 8b. Different from the gradual adsorption of POP-a, the POP-b was rapidly adsorbed on the CNT surface at the last 1 ns of the simulation. The interaction energy decreased from 3.2292 kcal mol^{-1} to −24.8783 kcal mol^{-1}, and the contact area increased from 60.3084 Å^2 to 331.0457 Å^2, which were similar to the final values of POP-a. Then the peptide was rearranged itself and then effective adsorption was begun at 8.35 ns. In this case, the residue Arg19 was adsorbed on the CNT and drove the Ser9, Ser15 and Asn12 to come close to the CNT. At the end of the simulation, the POP was mostly unfolded and exposed on the CNT surface.

3.7. Optimizing of the peptide

POP was found to be adsorbed on the SWCNT with several paths. However, it could not spread on the surface, but more readily to be assembled itself. Despite of the residues with aromatic rings were put close to the surface at the initial state, the SWCNT was mainly covered by the polar residues (green) with the interaction between long alkyl chain and the CNT. To optimize the peptide and discern the two kinds of residues, two peptides composed of aromatic residues only and long alkyl residues only were constructed. Threonine (Thr), Serine (Ser), Methionine (Met), Tryptophane (Trp) and Histidine (His) were the five typical adsorption residues found in the former study. The long alkyl chain-rich pep-1 was assembled with Thr, Ser and Met. And Trp and His were used to build the aromatic rings-rich pep-2.

As shown in Fig. 9, the adsorption time of pep-2 (blue bar) was longer than that of pep-1 (red bar). Moreover, the beginning time of the adsorption occurred earlier than that of pep-2. It was shown that pep-1 was more easily to be absorbed on SWCNT and more quickly to complete the adsorption than that of pep-2. With the analysis of MD simulation, six residues (Met2, Met5, Thr10, Met14, Thr19 and Met23) in the pep-1 system were found to be adsorbed on the CNT surface at the end of MD simulation. And the helix was unfolded to be two parts with the breaking of H-bond between Thr13 and Met17.Further analysis of the adsorption dynamics had found that the helix (1–13) turned right, however, the helix (17–24) turned left. Then it resulted in the breaking of H-bond and the transition of α-helix into π-helix. The long alkyl chains were found to be spread on the surface with all the H atoms exposed to CNT. Then combining the contact area and the CMW curves of pep-1 to the pep-2, it could be found that the rearrangement of pep-2 took much more time than that of pep-1 during the adsorption process.

For the pep-2 system, four residues (His18, Trp19, Trp21, and His22) were adsorbed on the surface in the final state. And the aromatic rings in these residues were found to be parallel to the CNT surface to form stable π–π interaction. It was discerned from the MD trajectory that the two aromatic rings gradually come close to CNT and then adsorb on the surface. Meanwhile, the aromatic rings were more readily to be parallel to the CNT surface. The aromatic ring of His18 was perpendicular to the surface in the initial state. It was adjusted to be parallel to the surface and the π–π interaction drove the ring to come close to CNT. At the same time, the aromatic ring of Trp19 was pulled onto the CNT to form new π–π interaction. Similarly, the adsorption of the indole ring in Trp21 induced the drop of His22. The distance of the ring center of imidazole in His18 and the CNT surface was displayed in Fig. 10a. At the initial

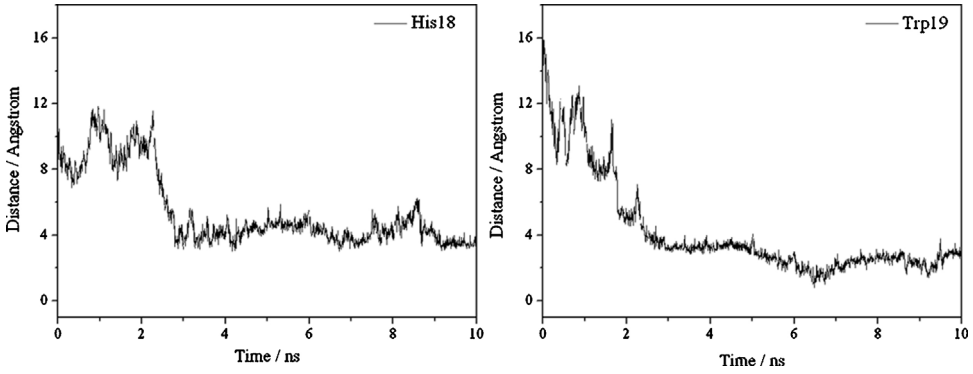

Fig. 10. Distance of (a) His18 and (b) Trp19 in pep-2 to the surface of SWCNT.

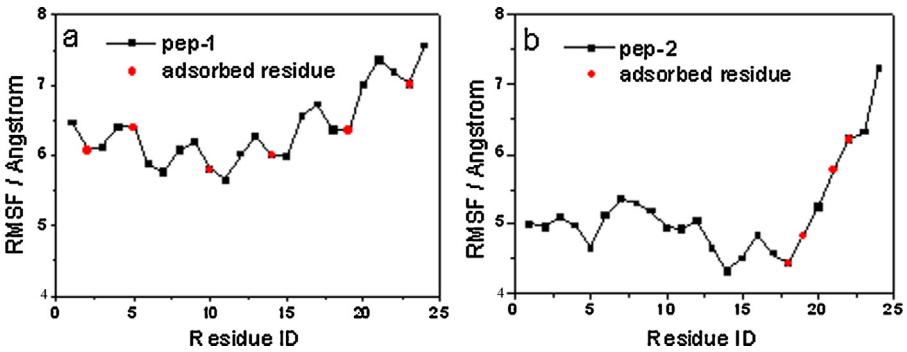

Fig. 11. RMSF of the backbone of (a) pep-1 and (b) pep-2 as a function of residue number. And the adsorbed residues were colored in red. (For interpretation of the references to colour in this figure legend, the reader is referred to the web version of this article.)

stage of simulation, the ring was 10.0 Å away from the CNT surface and it fluctuated between 7.8 and 11.8 Å for 2.2 ps. Then it dramatically dropped to 3.5 Å and kept stable around 4.0 Å at the end of simulation. The π–π stacking distance between the ring center of indole in Trp19 and the CNT surface was also shown in Fig. 10b. The distance of indole ring and surface was gradually decreased from 16.0 to 4.5 Å and then it was kept stable around 3.0 Å from 5.0 to 10.0 ns.

To illustrate the influence of the flexibility of each residues and peptides on the adsorption results, the root-mean-square fluctuation (RMSF) of the backbone of the two peptides were shown in Fig. 11. And the adsorbed residues at the end of the simulation were highlighted in red. As shown in Fig. 10a, the six adsorbed residues were distributed evenly in the pep-1. Moreover, the flexibility of the adsorbed residues (red points) was restricted by the interaction of residue and CNT. Then the RMSF values of these adsorbed residues were smaller than that of the neighbored residues. For pep-2, only four residues adsorbed on the CNT surface, and it was resulted by the rigidity of the peptide. Comparing the two RMSF curves, it could be found that the flexibility of pep-1 was larger than that of pep-2. The long alkyl-rich pep-1 was flexible enough to adjust the conformation of itself to adsorb on the CNT. However, the flexibility of pep-2 was restricted by the rigid aromatic rings.

The studies on nano-1 have shown that the residues with aromatic rings were more easily adsorbed onto the CNT. It was found in this work that the residues with long alkylene chain were also readily adsorbed on the CNT. The main driving forces of aromatic ring-rich and long alkylene chain-rich peptides were π–π stacking and VDW interaction, respectively. The aromatic rings close to the SWCNT were parallel to the surface, which could maximize the π–π interaction. Meanwhile, the alkylene chains were found to be spread on the surface and the hydrogen atoms of the long alkylene chain were found to be pointed to the SWCNT to stabilize the VDW interaction. With the flexibility of the long alkyl chain, the adsorption of pep-1 was more favorable than that of pep-2.

The time of the formation of stable adsorption in the new peptide systems were much shorter than that in the POP system. And the stable adsorption time of POP-a (Fig. 8a), POP-b (Fig. 8b), pep-1 and pep-2 (Fig. 9) were found to be 8.35 ns, 9.5 ns, 1.474 ns and 2.7 ns, respectively. It showed the predominant adsorption capability of newly designed peptides on SWCNT.

4. Conclusion

To design a kind of peptide for the functionalization and dispersion of the large-diameter SWCNT, a series of MD simulations based on insulin and WW domain were carried out in this work. The key adsorption residues were extracted in a stepwise manner. The residues with aromatic rings and long alkylene chains were found to be more effective in the adsorption of peptide onto the SWCNT surface. Further studies on two model peptides composed with aromatic rings or long alkylene chains were performed. And it was found that the predominant driving force of the aromatic residues and the alkylene-rich residues were π–π stacking and VDW forces, respectively. The adsorption manners of the two kinds of residues were different. Long alkylene chains were readily to spread on the surface to increase the VDW interaction. Yet the aromatic rings were rearranged to be parallel to the surface to maximize the π–π interaction. Moreover, it was also found that the flexibility of long alkyl chain could facilitate the adsorption on CNT. For proteins (insulin and WW domain), the adsorption on SWCNT was completed in a stepwise manner and it was restricted by the tertiary structure of protein. While the CNT was immersed in the peptide solution, it could be quickly wrapped by the functional peptides to be dispersed. Moreover, the peptide was easy to be adapted by the body, which could be used as a safe and facile non-covalent modification biomolecules for CNT.

Although the simulations achieved some reasonable results, there are still limitations in these simulations. Short time MD simulation could achieve the mete-stable state but it is probably not long enough to reach a truly equilibrium state and longer simulation are needed to get various system behaviors. And the wrapping stability of peptide-SWCNT composite should be tested by the experiments. Further study on the minimum and maximum sizes of peptide should be carried out to discern the wrapping function of peptide. This work might be helpful for the understanding of the adsorption dynamics of protein/peptide on SWCNT at atomic level and molecular design of non-covalent modification of low-dimensional carbon nanomaterials.

Acknowledgements

This work was financially supported by the National Natural Science Foundation of China (Grant No. 21003037) and the National Science Foundation of the Education Department of Henan Province (13A150085).

References

[1] H.K. Li, J.H. Huang, J.H. Lv, H.J. An, X.D. Zhang, Z.Z. Zhang, C.H. Fan, J. Hu, Nanoparticle PCR: Nanogold-assisted PCR with enhanced specificity, Angew. Chem. Int. Ed. 44 (2005) 5100–5103.
[2] R.F. Service, Is nanotechnology dangerous, Science 290 (2000) 1526–1527.
[3] K. Donaldson, R. Aitken, L. Tran, V. Stone, R. Duffin, G. Forrest, A. Alexander, Carbon nanotubes: a review of their properties in relation to pulmonary toxicology and workplace safety, Toxicol. Sci. 92 (2006) 5–22.
[4] N. Gilbert, Nanoparticle safety in doubt, Nature 460 (2009) 937.
[5] R. Saito, G. Dresselhaus, M.S. Dresselhaus, Physical Properties of Carbon Nanotubes, Imperial College Press, London, 1998.
[6] A. Bianco, K. Kostarlos, C.D. Partidos, M. Prato, Biomedical applications of functionalized carbon nanotubes, Chem. Commun. 5 (2005) 571–577.

[7] L. Lacerda, A. Bianco, M. Prato, K. Kostarelos, Carbon nanotubes as nanomedicines: from toxicology to pharmacology, Adv. Drug Deliver. Rev. 58 (2006) 1460–1470.
[8] W. Zhao, C. Song, P.E. Pehrsson, Water-soluble and optically pH-sensitive single-walled carbon nanotubes from surface modification, J. Am. Chem. Soc. 124 (2002) 12418–12419.
[9] K. Kurppa, H. Jiang, G.R. Szilvay, A.G. Nasibulin, E.I. Kauppinen, M.B. Linder, Controlled hybrid nanostructures through protein-mediated noncovalent functionalization of carbon nanotubes, Angew. Chem. 119 (2007) 6566–6569; K. Kurppa, H. Jiang, G.R. Szilvay, A.G. Nasibulin, E.I. Kauppinen, M.B. Linder, Controlled hybrid nanostructures through protein-mediated noncovalent functionalization of carbon nanotubes, Angew. Chem. Int. Ed. 46 (2007) 6446–6449.
[10] A. Bianco, J. Hoebeke, S. Godefroy, O. Chaloin, D. Pantarotto, J.P. Briand, S. Muller, M. Prato, C.D. Partidos, Cationic carbon nanotubes bind to CpG oligodeoxynucleotides and enhance their immunostimulatory properties, J. Am. Chem. Soc. 127 (2005) 58–59.
[11] V.C. Moore, M.S. Strano, E.H. Haroz, R.H. Hauge, J.L. Margrave, R.E. Smalley, J. Schmidt, Y. Talmon, Individually suspended single-walled carbon nanotubes in various surfactants, Nano. Lett. 3 (2003) 1379–1382.
[12] L.Y. Li, Y. Yang, G.L. Yang, X.M. Chen, B.S. Hsiao, B. Chu, J.E. Spanier, C.Y. Li, Patterning polyethylene oligomers on carbon nanotubes using physical vapor deposition, Nano. Lett. 6 (2006) 1007–1012.
[13] Y. Chen, H.P. Liu, T. Ye, J. Kim, C.D. Mao, DNA-directed assembly of single-wall carbon nanotubes, J. Am. Chem. Soc. 129 (2007) 8696–8697.
[14] S. Wang, E.S. Humphreys, S.Y. Chung, D.F. Delduco, S.R. Lustig, H. Wang, K.N. Parker, N.W. Rizzo, S. Subramoney, Y.M. Chiang, A. Jagota, Peptides with selective affinity for carbon nanotubes, Nat. Mater. 2 (2003) 196–200.
[15] S.S. Karajanagi, H. Yang, P. Asuri, E. Sellitto, J.S. Dordick, R.S. Kane, Protein-assisted solubilization of single-walled carbon nanotubes, Langmuir 22 (2006) 1392–1395.
[16] G.R. Dieckmann, A.B. Dalton, P.A. Johnson, J. Razal, J. Chen, G.M. Giordano, E. Munoz, I.H. Musselman, R.H. Baughman, R.K. Draper, Controlled assembly of carbon nanotubes by designed amphiphilic peptide helices, J. Am. Chem. Soc. 125 (2003) 1770–1777.
[17] A.B. Dalton, A. Ortiz-Acevedo, V. Zorbas, E. Brunner, W.M. Sampson, S. Collins, J.M. Razal, M.M. Yoshida, R.H. Baughman, R.K. Draper, I.H. Musselman, M. Jose-Yaca-man, G.R. Dieckmann, Controlled assembly of carbon nanotubes by designed amphiphilic peptide helices, Adv. Funct. Mater. 14 (2004) 1147–1151.
[18] V. Zorbas, A.L. Smith, A. Ortiz-Acevedo, H. Xie, A.B. Dalton, G.R. Dieckmann, R.K. Draper, R.H. Baughman, I.H. Mussel-man, Importance of aromatic content for peptide/single-walled carbon nanotube interactions, J. Am. Chem. Soc. 127 (2005) 12323–12328.
[19] V. Zorbas, A. Ortiz-Acevedo, A.B. Dalton, M.M. Yoshida, G.R. Die-ckmann, R.K. Draper, R.H. Baughman, M. Jose-Yacaman, I.H. Musselman, Preparation and characterization of individual peptide-wrapped single-walled carbon nanotubes, J. Am. Chem. Soc. 126 (2004) 7222–7227.
[20] C.C. Chiu, G.R. Dieckmann, S.O. Nielsen, Molecular dynamics study of a nanotube-binding amphiphilic helical peptide at different water/hydrophobic interfaces, J. Phys. Chem. B 112 (2008) 16326–16333.
[21] C.C. Chiu, G.R. Dieckmann, S.O. Nielsen, Role of peptide–peptide interactions in stabilizing peptide-wrapped single-walled carbon nanotubes: a molecular dynamics study, Peptide Sci. (2009) 156–163.
[22] G.H. Zuo, Q. Huang, G.h. Wei, R.H. Zhou, H.P. Fang, Plugging into proteins: Poisoning protein function by a hydrophobic nanoparticle, ACS. Nano. 4 (2010) 7508–7514.
[23] J.W. Shen, T. Wu, Q. Wang, Y. Kang, X. Chen, Adsorption of insulin peptide on charged single-walled carbon nanotubes: significant role of ordered water molecules, Chem. Phys. Chem. 10 (2009) 1260–1269.
[24] Y. Kang, Y.C. Liu, Q. Wang, J.W. Shen, T. Wu, W.J. Guan, On the spontaneous encapsulation of proteins in carbon nanotubes, Biomaterials 30 (14) (2009) 2807–2815.
[25] Y. Kang, Q. Wang, Y.C. Liu, J.W. Shen, T. Wu, Diameter selectivity of protein encapsulation in carbon nanotubes, J. Phys. Chem. B 114 (8) (2010) 2869–2875.
[26] M.J. Macias, M. Hyvonen, E. Baraldi, J. Schultz, M. Sudol, M. Saraste, H. Oschkinat, Structure of the WW domain of a kinase-associated protein complexed with a proline-rich peptide, Nature 382 (1996) 646–649.
[27] I.C. Yeh, G.H. Proc, Nucleic acid transport through carbon nanotube membranes, Natl. Acad. Sci. 101 (2004) 12177–12182.
[28] R.R. Johnson, A.T.C. Johnson, M.L. Klein, Probing the structure of DNA-carbon nanotube hybrids with molecular dynamics, Nano. Lett. 8 (2008) 69–75.
[29] J.W. Shen, T. Wu, Q. Wang, Y. Kang, Induced stepwise conformational change of human serum albumin on carbon nanotube surfaces, Biomaterial 29 (2008) 3847–3855.
[30] H. Gao, Y. Kong, D. Cui, C.S. Ozkan, Spontaneous insertion of DNA oligonucleotides into carbon nanotubes, Nano. Lett. 3 (2003) 471–473.
[31] E.J. Sorin, V.S. Pande, Nanotube confinement denatures protein helices, J. Am. Chem. Soc. 128 (2006) 6316–6317.
[32] H.J.C. Berendsen, J.P.M. Postma, W.F. van Gusteren, J. Hermans, Interaction models for water in relation to protein hydration, in: B. Pullman (Ed.), Intermolecular Forces, Reidel, Dordrecht, 1981, pp. 331–342.
[33] H.J.C. Berendsen, J.R. Grigera, T.P. Straatsma, The missing term in effective pair potentials, J. Phys. Chem. 91 (1987) 6269–6271.
[34] J.C. Phillips, R. Braun, W. Wang, J. Gumbart, E. Tajkhorshid, E. Villa, C. Chipot, R.D. Skeel, L. Kale, K. Schulten, Scalable molecular dynamics with NAMD, J. Comput. Chem. 26 (2005) 1781–1802.
[35] A.D. MacKerell Jr., D. Bashford, M. Bellott, R.L. Dunbrack Jr., J.D. Evan-seck, M.J. Field, S. Fischer, J. Gao, H. Guo, S. Ha, D. Joseph-McCarthy, L. Kuchnir, K. Kuczera, F.T.K. Lau, C. Mattos, S. Michnick, T. Ngo, D.T. Nguyen, B. Prodhom, W.E. Reiher III, B. Roux, M. Schlenkrich, J.C. Smith, R. Stote, J. Straub, M. Watanabe, J. Wi_rkiewicz-Kuczera, D. Yin, M. Kar-plus, All-atom empirical potential for molecular modeling and dynamics studies of proteins, J. Phys. Chem. B 102 (1998) 3586–3616.
[36] J.H. Walther, R. Jaffe, T. Halicioglu, P. Koumoutsakos, Carbon nanotubes in water: structural characteristics and energetics, J. Phys. Chem. B 105 (2001) 9980–9987.
[37] J.W. Shen, T. Wu, Q. Wang, H.H. Pan, Molecular simulation of protein adsorption and desorption on hydroxyapatite surfaces, Biomaterials 29 (2008) 513–532.
[38] X. Chen, T. Wu, Q. Wang, J.W. Shen, Shield effect of silicate on adsorption of protein onto silicon-doped hydroxyapatite (100) surface, Biomaterials 29 (2008) 2423–2432.
[39] H.J. Gao, Y. Kong, Simulation of DNA–nanotube interactions, Annu. Rev. Mater. Res. 34 (2004) 123–150.
[40] S. Ravichandran, J.D. Madura, J. Talbot, A Brownian dynamics study of the initial stages of hen egg-white lysozyme adsorption at a solid interface, J. Phys. Chem. B 105 (2001) 3610–3613.
[41] D.E. Shaw, P. Maragakis, K. Lindorff-Larsen, S. Piana, R.O. Dror, M.P. Eastwood, J.A. Bank, J.M. Jumper, J.K. Salmon, Y.B. Shan, W. Wriggers, Atomic-level characterization of the structural dynamics of proteins, Science 330 (2010) 341–346.
[42] A.B. Guliaev, S. Cheng, B. Hang, Protein dynamics via computational microscope, World J. Methodol. 2 (2012) 42–49.
[43] H.L. Zhou, T. Wu, X.L. Dong, Q. Wang, J.W. Shen, Adsorption mechanism of BMP-7 on hydroxyapatite (001) surfaces, Biochem. Biophys. Res. Commun. 361 (2007) 91–96.
[44] P. Bjelkmar, P. Laesson, M.A. Cuendet, B. Hess, E. Lindahl, Implementation of the CHARMM force field in GROMACS: analysis of protein stability effects from correction maps, virtual interaction sites, and water models, J. Chem. Theory Comput. 6 (2010) 459–466.
[45] Q.X. Mu, W. Liu, Y.H. Xing, H.Y. Zhou, Z.W. Li, Y. Zhang, L.H. Ji, F. Wang, Z.K. Si, B. Zhang, B. Yan, Protein binding by functionalized multiwalled carbon nanotubes is governed by the surface chemistry of both parties and the nanotube diameter, J. Phys. Chem. C 112 (2008) 3300–3307.
[46] C. Rajesh, C. Majumder, H. Mizuseki, Y. Kawazoe, A theoretical study on the interaction of aromatic amino acids with graphene and single walled carbon nanotube, J. Chem. Phys. 130 (2009) 124911–124917.
[47] Y.Z. Liu, C. Chipot, X.G. Shao, W.S. Cai, Edge effects control helical wrapping of carbon nanotubes by polysaccharides, Nanoscale 4 (2012) 2584–2589.
[48] A.C. Camproux, R. Gautier, P. Tuffery, A hidden markov model derived structural alphabet for proteins, J. Mol. Biol. 339 (3) (2004) 591–605.
[49] J. Maupetit, P. Derreumaux, P. Tuffery, A fast and accurate method for large-scale de novo peptide structure prediction, J. Comput. Chem. 31 (4) (2010) 726–738.
[50] J. Maupetit, P. Tuffery, P. Derreumaux, A coarse-grained protein force field for folding and structure prediction, Proteins 69 (2) (2007) 394–408.
[51] H. Kaur, A. Garg, G.P. Raghava, PEPstr: a de novo method for tertiary structure prediction of small bioactive peptides, Protein. Pept. Lett. 14 (7) (2007) 626–631.
[52] Z. Wang, J. Eickholt, J. Cheng, APOLLO: a quality assessment service for single and multiple protein models, Bioinformatics 27 (12) (2011) 1715–1716.
[53] J. Beaufays, L. Lins, A. Thomas, R. Brasseur, In silico predictions of 3D structures of linear and cyclic peptides with natural and non-proteinogenic residues, J. Pept. Sci. 18 (2012) 17–24.
[54] M.L. Connolly, Solvent-accessible surfaces of proteins and nucleic-acids, Science 221 (1983) 709–713.
[55] A.T. Macias, A.D. MacKerell, CH/π interactions involving aromatic amino acids: refinement of the CHARMM tryptophan force field, J. Comput. Chem. 26 (2005) 1452–1463.
[56] C.A. Hunter, J.K.M. Sanders, Dabco-metalloporphyrin binding: ternary complexes, host-guest chemistry and the measurement of pi–pi interactions, J. Am. Chem. Soc. 112 (1990) 5525–5534.
[57] G. Raffaini, F. Ganazzoli, Molecular dynamics simulation of the adsorption of a fibronectin module on a graphite surface, Langmuir 20 (2004) 3371–3378.
[58] G. Raffaini, F. Ganazzoli, Simulation study of the interaction of some albumin subdomains with a flat graphite surface, Langmuir 19 (2003) 3403–3412.
[59] G. Raffaini, F. Ganazzoli, Surface ordering of proteins adsorbed on graphite, J. Phys. Chem. B 108 (2004) 13850–13854.
[60] G. Raffaini, F. Ganazzoli, Molecular dynamics simulation of the adsorption of a fibronectin module on a graphite surface, Langmuir 20 (2004) 3371–3378.
[61] W. Humphrey, A. Dalke, K. Schulten, VMD: visual molecular dynamics, J. Mol. Graphics 14 (1996) 33–38.
[62] J. Zielkiewicz, Structural properties of water: comparison of the SPC, SPCE, TIP4P, and TIP5P models of water, J. Chem. Phys. 123 (2005) 104501–104506.
[63] W.L. Jorgensen, J. Chandrasekhar, J.D. Madura, Comparison of simple potential functions for simulating liquid water, J. Chem. Phys. 79 (1983) 926–935.
[64] S.S. Karajanagi, A.A. Vertegel, R.S. Kane, J.S. Dordick, Structure and function of enzymes adsorbed onto single-walled carbon nanotubes, Langmuir 20 (2004) 11594–11599.
[65] D. Dutta, S.K. Sundaram, J.G. Teeguarden, B. Joseph, L.S. Fifield, J.M. Jacobs, Adsorbed proteins influence the biological activity and molecular targeting of nano-materials, Toxicol. Sci. 100 (2007) 303–315.